Geometrically Invariant Image Watermarking Using Connected Objects and Gravity Centers

Hongxia Wang[a], Bangxu Yin[a], Linna Zhou[b]
[a] School of Information Science and Technology, Southwest Jiaotong University
Chengdu, 610031 - P.R.China
[b] University of International Relations, Beijing, 100091- P.R.China
[e-mail: hxwang@swjtu.edu.cn]

Received February 28, 2013; revised May 29, 2013; revised July27, 2013; revised September 16, 2013; accepted October 23, 2013; published November 29, 2013

Abstract

The design of geometrically invariant watermarking is one of the most challenging work in digital image watermarking research area. To achieve the robustness to geometrical attacks, the inherent characteristic of an image is usually used. In this paper, a geometrically invariant image watermarking scheme using connected objects and gravity center is proposed. First, the gray-scale image is converted into the binary one, and the connected objects according to the connectedness of binary image are obtained, then the coordinates of these connected objects are mapped to the gray-scale image, and the gravity centers of those bigger objects are chosen as the feature points for watermark embedding. After that, the line between each gravity center and the center of the whole image is rotated an angle to form a sector, and finally the same version of watermark is embedded into these sectors. Because the image connectedness is topologically invariant to geometrical attacks such as scaling and rotation, and the gravity center of the connected object as feature points is very stable, the watermark synchronization is realized successfully under the geometrical distortion. The proposed scheme can extract the watermark information without using the original image or template. The simulation results show the proposed scheme has a good invisibility for watermarking application, and stronger robustness than previous feature-based watermarking schemes against geometrical attacks such as rotation, scaling and cropping, and can also resist common image processing operations including JPEG compression, adding noise, median filtering, and histogram equalization, etc.

Keywords: Digital image watermarking, geometrical distortion, connected object, gravity center, robustness

This research was supported by the National Natural Science Foundation of China (NSFC) under the grant nos. 61170226, 61170175 the Fundamental Research Funds for the Central Universities under the grant nos. SWJTU11CX047 and SWJTU12ZT02, the Young Innovative Research Team of Sichuan Province under the grant no. 2011JTD0007, and Chengdu Science and Technology program under the grant no. 12DXYB214JH-002.

http://dx.doi.org/10.3837/tiis.2013.11.020

1. Introduction

Recently, with the development of computer network and information technology, lots of digital multimedia data are stored, transmitted and distributed through Internet, which lead to illegal copy, manipulation or use without any control for the electronic content. As an important information security technique, the digital watermarking has become an efficient way to the copyright protection and content authentication [1]. For different purposes, digital watermarking can be broadly classified into two categories: robust watermarking and fragile watermarking. The former is used to protect ownership of the digital media, while the latter is used to authenticate the integrity and verity of the digital content [2]. The robust watermarking is generally designed to withstand various attacks. The attacks in watermarking systems can be roughly classified into signal processing attacks and geometrical attacks [3]. Traditional signal processing attacks include JPEG compression, adding noise, histogram equalization, image filtering, etc., while typical geometrical attacks consist of rotation, scaling, translation (RST), cropping, etc. Signal processing attacks act by reducing the watermark energy so that the watermark may disappear after attacks. By comparison, geometrical attacks can destroy the synchronization between watermark embedding and extraction. In other words, the position of the watermark has changed although it still exists in the image. Many existing robust watermarking techniques have successfully resisted traditional signal processing attacks [4] [5] [6]. However, the ability to resist geometrical attacks is still one of the most challenging issues [7]. Current geometrically invariant watermarking techniques include template-based embedding, invariant-transform domain (e.g. Fourier-Mellin transform) embedding, and feature-based embedding.

In [8], S. Pereira *et al* proposed a geometrically invariant watermarking algorithm based on polar maps for the accurate and efficient recovery of the template in an image which had undergone an arbitrary linear transformation. The main idea consists of adding structure to the template, and the experimental results demonstrate the robustness against common image processing operations such as JPEG compression, rotation, scaling, and aspect ratio changes. However, the template-based watermarking schemes immune to rotation, scale and translation (RST) attacks are not secure because the fixed structure of the template may be removed and destroyed easily. In [9], A. R. Manuel *et al* improved the algorithms belonging to the family of those exploiting the template with a regular structure by using the Levenberg-Marquardt's method for nonlinear least-squares estimation, and an estimate of the affine synchronization parameters after geometrical distortions could be obtained. Another common method is based on invariant-transform domains to design geometrically invariant watermarking schemes. RST resilient watermarking for image exploiting Fourier-Mellin transform was proposed in [10]. But the scheme is less effective to other types of geometrical distortion such as local warping due to the interpolation and quantization effect of inverse DFT transform.

Robustness can be also achieved by applying the geometrically invariant feature. Up to now, feature-based embedding has been widely applied in geometrically invariant watermarking schemes. In [11], an statistical feature-based geometrically invariant watermarking scheme was presented, which can resist both geometrical attacks and signal processing attacks Unfortunately, this scheme cannot resist image cropping. To tackle the issue of geometrical distortions, a robust blind watermarking in quaternion Fourier transform domain was proposed in [12]. In this scheme, the fast quaternion Fourier transform is performed on the image block, and some low-order pseudo-Zernike moments of the real

quaternion Fourier transform coefficient matrix are computed, which are regarded as the effective feature vectors. Experimental results show the robustness to common image processing operations and geometrical distortions. However, this scheme is not very robust against median filtering and light lowering for texture image. In addition, the computational complexity is slightly high for least squares support vector machine training and pseudo-Zernike moments computation. In [13], I. Nasir *et al* adopted a feature extraction method based on end-stopped wavelets to extract significant geometry preserving feature points, which was robust against various types of common image processing and geometrical attacks. Ref. [14] developed a watermarking method to jointly enhance the robustness and security of feature-based image watermarking schemes. The controlled randomization is incorporated in determining the feature regions of an image for mitigating the leakage of secret information. The experimental results of robustness evaluation demonstrate that the method can effectively resist various attacks, including noise-like signal processing and geometrical distortions. In [15], Niu *et al* presented a geometrically invariant watermarking using the invariant centroid theory and the support vector regression (SVR). The geometrically invariant space is constructed based on color image normalization, and the watermark is embedded into host color image by modifying the low frequency nonsubsampled contourlet transform coefficients. The watermark can be blindly extracted and automatically re-synchronized under geometrical distortions. However, SVR training process expends a lot of time to get an optimal regression function, which drops the computational efficiency. In addition, a robust digital color image watermarking algorithm which combines color image feature point extraction and shape image normalization was proposed in [16] The feature point extraction method called Mexican Hat wavelet scale interaction is used to select the points which can survive a variety of geometry attacks.

In this paper, we develop a geometrically invariant watermarking scheme based on the connected object and gravity center of an image aiming at better performances. This paper is organized as follows: Section 2 overviews the connected object and gravity center of the image. Section 3 describes the proposed geometrically invariant watermarking for digital images. In Section 4, we theoretically analyze the geometrical invariability. Simulation results and comparison with previous works are shown in Section 5. Finally, we draw our conclusions in Section 6.

2. Connected Object and Gravity Center of Digital Image

2.1 Connected Object

The connectedness is used to describe the regions and boundaries of an image. To identify connected objects in a digital image, we need to locate groups of the correlative pixels that are ‘connected’ to each other. In fact, the connected objects growing of an image according to the connectedness is a kind of feature-based image segmentation process that partitions a digital image into lots of disjoint regions. A region is a connected set of pixels, in which all the pixels are adjacent or touching.

For many operations, distinguishing connected objects depends on the convention used to decide whether pixels are connected. Typically, there are two types of connectedness patterns: 8-connectedness and 4-connectedness. For 8-connectedness pattern, all of the pixels that touch the pixel of interest are considered, including those on the diagonals. Thus, each pixel would have eight neighbors. For 4-connectedness pattern, the pixels along the diagonals are not considered, and each pixel has only four neighbors. Therefore, the selection of connectedness patterns affects the number of connected objects.

In a binary image, a pixel can either have a value of '1' as the object or '0' as the background, and the pixels with value '1' are white while value '0' are black. For example, the binary matrix A represents the binary image shown in **Fig. 1(a)**. If we adopt the 8-connectedness pattern, the original binary image will consist of five connected objects shown in **Fig. 1(b)**. But if we adopt the 4-connectedness pattern, there will be six connected objects shown in **Fig. 1(c)**.

$$A = \begin{bmatrix} 0&0&0&0&0&0&0&0&0&0&0&0&0&0&0 \\ 0&0&0&0&0&0&1&1&1&1&0&1&0&1&0 \\ 0&0&0&0&0&0&1&1&0&1&1&1&0&0&0 \\ 0&0&0&0&0&1&1&1&1&1&0&0&0&0&0 \\ 0&0&0&0&0&0&0&0&0&0&0&0&0&0&0 \\ 0&0&0&0&0&0&0&0&0&0&0&0&0&0&0 \\ 0&1&1&1&1&1&0&0&0&0&0&1&1&1&0 \\ 0&1&0&0&1&0&0&0&0&0&1&0&1&1&0 \\ 0&1&1&1&1&0&0&0&0&0&0&0&1&1&0 \\ 0&1&1&1&0&0&0&0&0&0&0&0&0&0&0 \\ 0&0&0&1&1&1&0&0&0&0&0&0&0&0&0 \\ 0&0&0&0&0&0&0&0&0&1&1&1&0&0&0 \\ 0&0&0&0&0&0&0&0&0&1&1&1&0&0&0 \\ 0&0&0&0&0&0&0&0&0&1&1&1&0&0&0 \\ 0&0&0&0&0&0&0&0&0&0&0&0&0&0&0 \end{bmatrix} \quad (1)$$

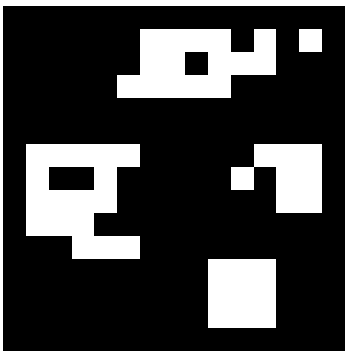

$$\begin{bmatrix} 0&0&0&0&0&0&0&0&0&0&0&0&0&0&0 \\ 0&0&0&0&0&0&2&2&2&2&0&2&0&5&0 \\ 0&0&0&0&0&0&2&2&0&2&2&2&0&0&0 \\ 0&0&0&0&0&2&2&2&2&2&0&0&0&0&0 \\ 0&0&0&0&0&0&0&0&0&0&0&0&0&0&0 \\ 0&0&0&0&0&0&0&0&0&0&0&0&0&0&0 \\ 0&1&1&1&1&1&0&0&0&0&4&4&4&0 \\ 0&1&0&0&1&0&0&0&0&0&4&0&4&4&0 \\ 0&1&1&1&1&0&0&0&0&0&0&0&4&4&0 \\ 0&1&1&1&0&0&0&0&0&0&0&0&0&0&0 \\ 0&0&0&1&1&1&0&0&0&0&0&0&0&0&0 \\ 0&0&0&0&0&0&0&0&0&3&3&3&0&0&0 \\ 0&0&0&0&0&0&0&0&0&3&3&3&0&0&0 \\ 0&0&0&0&0&0&0&0&0&3&3&3&0&0&0 \\ 0&0&0&0&0&0&0&0&0&0&0&0&0&0&0 \end{bmatrix}$$

$$\begin{bmatrix} 0&0&0&0&0&0&0&0&0&0&0&0&0&0&0 \\ 0&0&0&0&0&0&2&2&2&2&0&2&0&6&0 \\ 0&0&0&0&0&0&2&2&0&2&2&2&0&0&0 \\ 0&0&0&0&0&2&2&2&2&2&0&0&0&0&0 \\ 0&0&0&0&0&0&0&0&0&0&0&0&0&0&0 \\ 0&0&0&0&0&0&0&0&0&0&0&0&0&0&0 \\ 0&1&1&1&1&1&0&0&0&0&5&5&5&0 \\ 0&1&0&0&1&0&0&0&0&0&4&0&5&5&0 \\ 0&1&1&1&1&0&0&0&0&0&0&0&5&5&0 \\ 0&1&1&1&0&0&0&0&0&0&0&0&0&0&0 \\ 0&0&0&1&1&1&0&0&0&0&0&0&0&0&0 \\ 0&0&0&0&0&0&0&0&0&3&3&3&0&0&0 \\ 0&0&0&0&0&0&0&0&0&3&3&3&0&0&0 \\ 0&0&0&0&0&0&0&0&0&3&3&3&0&0&0 \\ 0&0&0&0&0&0&0&0&0&0&0&0&0&0&0 \end{bmatrix}$$

(a) Binary image **(b)** By 8-connectedness **(c)** By 4-connectedness

Fig. 1. An example of connected objects

2.2 Gravity Center

The gravity center is calculated by the low order moments of the image. The two-dimensional moment can be directly used in the interested regions and need not to separate it from the whole image. High order moments are more sensitive to noise, while the low order moments are insensitive to noise and quantization errors, which is beneficial to the characterization of

collectivity for the regions.

The 2-D (p+q)th order origin moment of a continuous image Ω is defined as [17]

$$M_{pq} = \int_{\Omega} x^p y^q f(x, y) dxdy, \ (p, q=0, 1, 2, \dots) \tag{2}$$

where $f(x, y)$ represents the gray-level value at location (x, y). For digital image, the integrals are replaced by summations as follows:

$$M_{pq} = \sum_{(x,y)\in\Omega} x^p y^q f(x, y) \tag{3}$$

The gravity center $G(g_x, g_y)$ of the image is easily defined in terms of the zero-order moment and first-order moments as follows [18]:

$$g_x = M_{10} / M_{00}, \qquad g_y = M_{01} / M_{00} \tag{4}$$

where the zero-order moment M_{00} represents the area of the image clearly. Similarly, the gravity center of the connected object can be work out when the set Ω is replaced with the connected object.

3. Proposed Geometrically Invariant Watermarking Scheme

3.1 Moderate Connected Objects

In order to resist the geometrical attacks such as rotation and scaling, watermark embedding is based on the inherent characteristics of image in general. In this paper, we use the connected objects as a characteristic, because the connected object of an image possesses topological invariability from morphology theory. The number of connected objects is invariable to the geometrical distortion of an image from a theoretical point of view, unless the image is torn up. However, if we directly use the original gray-scale image to convert to the binary version, the generated connected objects will contain the very big or small objects. For a very big connected object, only one gravity center can be obtained in a quite large area, while the gravity center of a very small connected object is instable. As well known, the median filtering is a simple and very effective noise removal filtering process. It usually causes significant loss of the detail and small objects in the image. Based on this performance, we can use median filtering to smooth original gray-scale image and remove some details and small objects. After that, the generated connected objects are more moderate. For the filter window S_{xy}, after performing the median filtering, each output pixel $\bar{f}(x, y)$ contains the median value in the S_{xy} neighborhood around the corresponding pixel in the input image $f(x, y)$, namely

$$\bar{f}(x, y) = \underset{(x,y)\in S_{xy}}{medfilt}\{f(x, y)\} \tag{5}$$

Then, we convert $\bar{f}(x, y)$ into binary $\bar{f}_b(x, y)$ by a threshold T_1 as following

$$\bar{f}_b(x, y) = \begin{cases} 1, & \bar{f}(x, y) / \max\{\bar{f}(x, y)\} > T_1 \\ 0, & \bar{f}(x, y) / \max\{\bar{f}(x, y)\} \le T_1 \end{cases} \tag{6}$$

By this way, the background and object pixels have gray levels grouped into two dominant modes by the threshold $T_1 \in [0,1]$. The pixels signed '1' is corresponding to the objects, whereas those pixels signed '0' is corresponding to the background. Suppose that the area size of the moderate connected objects is limited in the interval $[C_1, C_2]$, the pixels number in a

connected object will be $N\{\bar{f}(x,y) > \max\{\bar{f}(x,y)\} \cdot T_1\} \in [C_1, C_2]$. If the principal density of $\bar{f}(x,y)$ is the Gaussian distributing with mean μ and variance σ. Then, the optimal threshold T_1 satisfies [18]:

$$T_1 = \frac{\mu_1 + \mu_2}{2} + \frac{\sigma^2}{\mu_1 - \mu_2} \ln[P_2 / P_1] \tag{7}$$

Here, P_1 and P_2 are the probabilities of the object pixels and background pixels, respectively, and μ_1 and μ_2 are the means of the Gaussian distributing for two types of pixels. Suppose the variances of two types of pixels are all σ^2. Thus, the moderate connected object can be obtained by selecting the optimal threshold T_1.

3.2 Feature Points for Watermark Embedding

The generated connected objects' coordinates are mapped to the gray-scale image, thus the original image is also composed of lots of connected objects. Let Ω_i (i=1,2, …, u) represent u connected objects in the gray-scale image, and $N(\Omega_i)$ represent the number of pixels in each object. We define another threshold T_2 satisfying

$$\min_i\{N(\Omega_i)\} \le T_2 \le \max_i\{N(\Omega_i)\}, \ (i=1,2, \ldots, u) \tag{8}$$

The threshold T_2 partly controls the number of connected objects. **Fig. 2** shows some test images, and **Fig. 3** shows the number of connected objects of these images with different threshold T_2 under median filtering window 5×5 and 15×15, respectively. The larger T_2, the less number of connected objects will be. This leads to the bigger connected objects are held. In general, the gravity centers of bigger connected objects are stable. To obtain stable gravity centers as the feature points, we select the number of connected objects is 3~11. From **Fig. 3**, we see that when the number of connected objects for most of the images is 3~11 under different filtering windows, T_2 value falls into the interval [140, 300]. So the appropriate T_2 value should be in the interval [140, 300] according to the experiment results.

(a) Lena **(b)** Barbara **(c)** Boat **(d)** Pepper **(e)** Airplane

Fig. 2. Test images

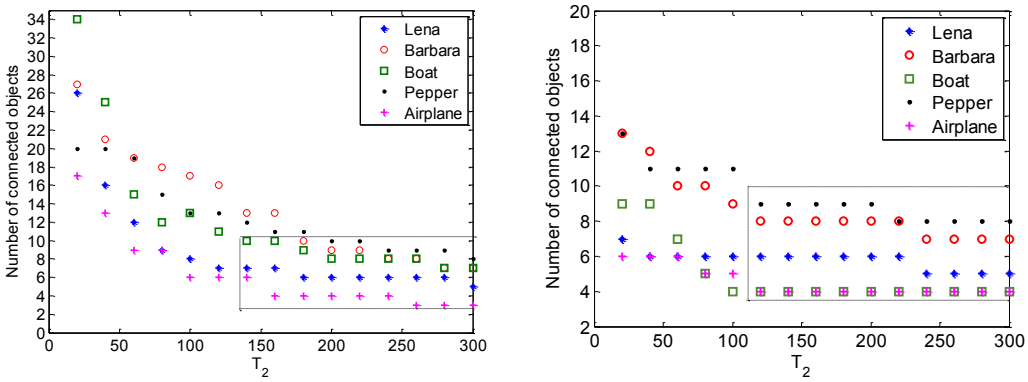

(a) Median filtering window 5×5 (b) Median filtering window 15×15

Fig. 3. Number of connected objects with different threshold T_2 under median filtering

To obtain stable feature points, we choose those bigger objects satisfying $N(\Omega_i) \geq T_2$ to calculate their gravity centers as the feature points $M_i(m_x^i, m_y^i)$ for watermark embedding as bellows

$$m_x^i = \int_{\Omega_i | N(\Omega_i) \geq T_2} xf(x,y)dxdy \Big/ \int_{\Omega_i | N(\Omega_i) \geq T_2} f(x,y)dxdy \tag{9}$$

$$m_y^i = \int_{\Omega_i | N(\Omega_i) \geq T_2} yf(x,y)dxdy \Big/ \int_{\Omega_i | N(\Omega_i) \geq T_2} f(x,y)dxdy \tag{10}$$

For each irregular connected object Ω_i, since

$$\int_{\Omega_i | N(\Omega_i) \geq T_2} xf(x,y)dxdy \Big/ \int_{\Omega_i | N(\Omega_i) \geq T_2} f(x,y)dxdy \in [\min\{x\}, \max\{x\}] \tag{11}$$

$$\int_{\Omega_i | N(\Omega_i) \geq T_2} yf(x,y)dxdy \Big/ \int_{\Omega_i | N(\Omega_i) \geq T_2} f(x,y)dxdy \in [\min\{y\}, \max\{y\}] \tag{12}$$

So if the connected object Ω_i is convex, the location of the feature points M_i will fall into the inside of the connected object, otherwise the feature points will fall into either the inside or outside of the concave connected objects.

3.3 Watermark Embedding

Firstly, the generated connected objects are sorted in descending order according to the number of pixels in each connected object. The connected objects including maximal number of pixels is at the forefront of the sorting result, and is the biggest connected object. According to T_2, we select anterior v bigger connected objects whose corresponding gravity centers $G_i (i = 1,2,\cdots,v)$ are worked out. Assume the center of the whole image is C. As shown in **Fig. 4**, let $\overrightarrow{CG_i}$ (i=1,2,…, v) be the starting radial, and its rotating α degree forms a sector. Then, we embed the same version of watermarks into each sector. The detailed watermark embedding method is as follows. First, We divide equally each sector into L parts using $L-1$ straight lines. Adding two angle lines, there will be total $L+1$ lines used for embedding watermark information in a sector, and then the length of the radial line $\overrightarrow{CG_i}$ is as the reference

length L_{ref}. For watermarking synchronization purpose, we use $\overrightarrow{cc_i}$ as the starting line, and equally embed N watermark bits on each line. Thus, the distance between two adjacent embedding points is L_{ref}/N. Thus, each sector will accommodate total $(L+1)N$ watermark bits. Because the watermark embedded into each sector is identical, so the distribution of watermark bits is thick for the sector with smaller area, while for those with bigger area, is sparse.

In general, the occurrence probability that two sectors overlap each other is very small. The cause is that the gravity centers of several bigger connected objects are used to form sectors, thus the distribution of these gravity centers is sparse, and it is not easy to make two sectors formed by these gravity centers overlapping.To avoid the small probability event that sectors are overlapped, we adopt the following method. If any sector i created from gravity center G_i (i = 1, 2, …, v) overlaps one of its previous sectors 1, 2, …, $i-1$, the gravity center G_i is just discarded and a new gravity center G_{v+1} is added whenever there are some gravity centers not yet been added.

In each embedding point, we note the gray-scale value $f \in Z$, and $0 \le f \le 255$, and use the odd-even quantization method to embed the watermark bit w_i, i=1,2,…, $(L+1)N$ into an image as follows:

When $w_i = 0$, the watermarked gray-scale value f_w satisfy

$$f_w = \begin{cases} \lfloor f/\Delta \rfloor \times \Delta + \lfloor \Delta/2 \rfloor, & \text{if } \lfloor f/\Delta \rfloor \bmod 2 = 0 \\ (\lfloor f/\Delta \rfloor - 1) \times \Delta + \lfloor \Delta/2 \rfloor, & \text{if } \lfloor f/\Delta \rfloor \bmod 2 = 1 \\ & \text{and } f \in [\lfloor f/\Delta \rfloor \times \Delta, \lfloor f/\Delta \rfloor \times \Delta + \lfloor \Delta/2 \rfloor) \\ (\lfloor f/\Delta \rfloor + 1) \times \Delta + \lfloor \Delta/2 \rfloor, & \text{if } \lfloor f/\Delta \rfloor \bmod 2 = 1 \text{ and } (\lfloor f/\Delta \rfloor + 1) \times \Delta + \lfloor \Delta/2 \rfloor \le 255 \\ & \text{and } f \in [\lfloor f/\Delta \rfloor \times \Delta + \lfloor \Delta/2 \rfloor, \lfloor f/\Delta \rfloor \times \Delta + \Delta) \\ (\lfloor f/\Delta \rfloor - 1) \times \Delta + \lfloor \Delta/2 \rfloor, & \text{if } \lfloor f/\Delta \rfloor \bmod 2 = 1 \text{ and } (\lfloor f/\Delta \rfloor + 1) \times \Delta + \lfloor \Delta/2 \rfloor > 255 \\ & \text{and } f \in [\lfloor f/\Delta \rfloor \times \Delta + \lfloor \Delta/2 \rfloor, \lfloor f/\Delta \rfloor \times \Delta + \Delta) \end{cases} \tag{13}$$

When $w_i = 1$, then the watermarked gray-scale value f_w satisfy

$$f_w = \begin{cases} \lfloor f/\Delta \rfloor \times \Delta + \lfloor \Delta/2 \rfloor, & \text{if } \lfloor f/\Delta \rfloor \bmod 2 = 1 \\ \Delta, & \text{if } \lfloor f/\Delta \rfloor \bmod 2 = 0 \text{ and } f < \lfloor \Delta/2 \rfloor \\ (\lfloor f/\Delta \rfloor - 1) \times \Delta + \lfloor \Delta/2 \rfloor, & \text{if } \lfloor f/\Delta \rfloor \bmod 2 = 0 \text{ and } f \ge \lfloor \Delta/2 \rfloor \\ & \text{and } f \in [\lfloor f/\Delta \rfloor \times \Delta, \lfloor f/\Delta \rfloor \times \Delta + \lfloor \Delta/2 \rfloor) \\ (\lfloor f/\Delta \rfloor + 1) \times \Delta + \lfloor \Delta/2 \rfloor, & \text{if } \lfloor f/\Delta \rfloor \bmod 2 = 0 \text{ and } (\lfloor f/\Delta \rfloor + 1) \times \Delta + \lfloor \Delta/2 \rfloor \le 255 \\ & \text{and } f \in [\lfloor f/\Delta \rfloor \times \Delta + \lfloor \Delta/2 \rfloor, \lfloor f/\Delta \rfloor \times \Delta + \Delta) \\ (\lfloor f/\Delta \rfloor - 1) \times \Delta + \lfloor \Delta/2 \rfloor, & \text{if } \lfloor f/\Delta \rfloor \bmod 2 = 0 \text{ and } (\lfloor f/\Delta \rfloor + 1) \times \Delta + \lfloor \Delta/2 \rfloor > 255 \\ & \text{and } f \in [\lfloor f/\Delta \rfloor \times \Delta + \lfloor \Delta/2 \rfloor, \lfloor f/\Delta \rfloor \times \Delta + \Delta) \end{cases} \tag{14}$$

where $\lfloor \bullet \rfloor$ denotes the floor function. $\Delta > 0$ is quantization step, which controls the watermark strength and can be set reasonably by the users. In general, the larger Δ will result in stronger robustness, while the quality of the watermarked image is degraded. So the selection of Δ values should be a reasonable trade-off between the perceptual transparency and the robustness. Consequenctly, to achieve this goal, the magnitude of the modified

gray-scale value should locate at the middle of the quantization interval. In generally, the more suitable values of Δ are in the interval [15, 23] according to the experiment results.

For example, we set the quantization step Δ =20, and assume the watermark bit 0 is embedded into the pixel point with gray-scale value f = 242. Due to $\lfloor 242/20 \rfloor \bmod 2 = 0$, the watermarked gray-scale value will be $f_w = \lfloor 242/20 \rfloor \times 20 + \lfloor 20/2 \rfloor = 250$ according to Eq.(13). However, if the watermark bit 0 is embedded into another gray-scale value f = 135, due to $\lfloor 145/20 \rfloor \bmod 2 = 1$ and $145 \in [\lfloor 145/20 \rfloor \times 20, \lfloor 145/20 \rfloor \times 20 + \lfloor 20/2 \rfloor)$, the watermarked gray-scale value will be $f_w = (\lfloor 145/20 \rfloor - 1) \times 20 + \lfloor 20/2 \rfloor = 130$ according to Eq. (13). Similarly, the embedding process of watermark bit 1 is similar to that of watermark bit 0 according to Eq. (14).

Now we describe an example of the underflow and overflow about the value of f_w. Assume the watermark bit 1 is embedded into the pixel point with gray-scale value f = 8. Due to $\lfloor 8/20 \rfloor \bmod 2 = 0$ and $8 < \lfloor \Delta/2 \rfloor$, the underflow would happen, and the watermarked gray-scale value will be $f_w = \Delta = 20$ according to Eq.(14). On the contrary, when f = 240, due to $\lfloor 240/20 \rfloor \bmod 2 = 0$ and $(\lfloor 240/20 \rfloor + 1) \times 20 + \lfloor 20/2 \rfloor > 255$, the overflow would happen, and the watermarked gray-scale value will be $f_w = (\lfloor 240/20 \rfloor - 1) \times 20 + \lfloor 20/2 \rfloor = 230$ according to Eq.(14).

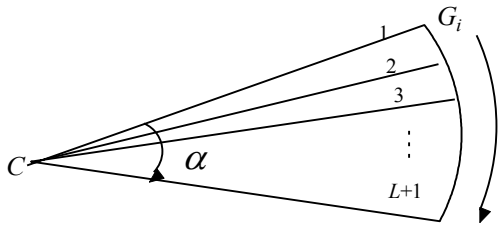

Fig. 4. Sector formed by the gravity center of connected object

3.4 Watermark Extracting

In the watermark retrieval process, first, we convert the gray-scale image into the binary one, and then obtain the moderate connected objects based on the median filtering and the connectedness technique. According to the threshold T_2, we can calculate the gravity centers of bigger connected objects used to embed watermark information. Like the watermark embedding process, several sectors are generated for watermark embedding. In each sector, we can extract a watermark version on $L+1$ lines. Because we use the center of the whole image and the gravity centers of connected objects as the feature points for watermark embedding in each sector, which is geometrically invariant, no matter how the image is rotated, scaled and translated, the watermark will be synchronized. The watermark $W' = \{w'_1, w'_2, \cdots \quad \in \{0,1\}\}$ is extracted as follows

$$w'_i = \begin{cases} 0, & \lfloor f_w / \Delta \rfloor \bmod 2 = 0 \\ 1, & \lfloor f_w / \Delta \rfloor \bmod 2 = 1 \end{cases} \tag{15}$$

where f_w denotes the watermarked gray-scale value. According to quantization method, when the difference between quantized gray-scale values and the original ones varies within $[-\Delta/2, \Delta/2)$, watermark bits will be correctly extracted, and the robustness is ensured.

4. Geometrical Invariability Analysis

The connected objects growing of an image according to the connectedness is a kind of feature-based image segmentation process that partitions a digital image into lots of disjoint regions. In addition, the gravity center of the connected object has the property of geometrically invariant. Based on the fact that connectedness and the gravity center are all geometrical invariability, the watermark can survive under geometrical attacks.

4.1 Rotation

After a rotation by an angle θ about the origin, the first-order moments are given by

$$\begin{aligned} M_{10}^r &= \sum_{(x,y)\in\Omega}(x\cos\theta + y\sin\theta)f(x,y) \\ &= M_{10}\cos\theta + M_{01}\sin\theta \end{aligned}$$

$$\begin{aligned} M_{01}^r &= \sum_{(x,y)\in\Omega}(y\cos\theta - x\sin\theta)f(x,y) \\ &= M_{01}\cos\theta - M_{10}\sin\theta \end{aligned}$$

and the zero-order moment $M_{00}^r = M_{00}$. So after rotating with an angle θ, the gravity center is changed as

$$g_x^r = M_{10}^r / M_{00}^r = g_x\cos\theta + g_y\sin\theta,\ g_y^r = M_{01}^r / M_{00}^r = g_y\cos\theta - g_x\sin\theta \tag{16}$$

Namely

$$\begin{bmatrix} g_x^r \\ g_y^r \end{bmatrix} = \begin{bmatrix} \cos\theta & \sin\theta \\ -\sin\theta & \cos\theta \end{bmatrix}\begin{bmatrix} g_x \\ g_y \end{bmatrix} \tag{17}$$

4.2 Scaling

After scaling with a factor α in the x-direction and β in the y-direction, the size of the image (object) is correspondingly changed. Let Ω^s represent the scaled image (object), then the first-order moments after scaling are given by

$$\begin{aligned} M_{10}^s &= \sum_{(x,y)\in\Omega^s} xf(x/\alpha, y/\beta) \\ &= \alpha^2\beta \sum_{(x/\alpha,y/\beta)\in\Omega}(x/\alpha)f(x/\alpha, y/\beta) \\ &= \alpha^2\beta M_{10} \end{aligned}$$

Similarly,

$$\begin{aligned} M_{01}^s &= \sum_{(x,y)\in\Omega^s} y\, f(x/\alpha, y/\beta) \\ &= \alpha\beta^2 M_{01} \end{aligned}$$

In addition, the zero-order moment $M_{00}^s = \alpha\beta M_{00}$. So the relation of gravity center between before and after scaling is

$$g_x^s = M_{10}^s / M_{00}^s = \alpha g_x,\ g_y^s = M_{01}^s / M_{00}^s = \beta g_y \tag{18}$$

Namely

$$\begin{bmatrix} g_x^s \\ g_y^s \end{bmatrix} = \begin{bmatrix} \alpha & 0 \\ 0 & \beta \end{bmatrix} \begin{bmatrix} g_x \\ g_y \end{bmatrix} \tag{19}$$

4.3 Translation

After translation of coordinates shifted in position Δx in the x-direction and Δy in the y-direction, the first-order moments are given by

$$\begin{aligned} M_{10}^t &= \sum_{(x,y)\in\Omega} (x+\Delta x) f(x,y) \\ &= M_{10} + \Delta x M_{00} \\ M_{01}^t &= \sum_{(x,y)\in\Omega} (y+\Delta y) f(x,y) \\ &= M_{01} + \Delta y M_{00} \end{aligned}$$

and the zero-order moment $M_{00}^t = M_{00}$. So the relation of gravity center between before and after translations is

$$g_x^t = M_{10}^t / M_{00}^t = g_x + \Delta x,\ g_y^t = M_{01}^t / M_{00}^t = g_y + \Delta y \tag{20}$$

From above analysis, we see the gravity center of an image (object) is invariant under RST transform.

To further explain that the proposed scheme is invariant after scaling, rotation and translation, we show a sketch map of the watermark embedding locations in **Fig. 5**. From **Fig. 5(a)**, there are five sectors are formed. The points in each sector are the watermark embedding locations, which are obtained according to the gravity centers based on the connected objects content. Therefore, the straight line $\overrightarrow{\omega\omega_i}$ (i=1,2,3,4,5) between the center of the whole image and the gravity center of each connected object rotates, scales and translates synchronously with the whole image. Consequently, the watermark embedding points can be find correctly after geometrical attacks to the watermarked image. For example, **Fig. 5 (b)** shows the watermark embedding points after rotating a degree. From **Fig. 5 (b)**, we see the watermark embedding points can be ratated adptively a degree with the whole image. **Fig. 5 (c)** and **(d)** show the watermark embedding points after scaling with factors 0.5 and 1.5, respectively. From **Fig. 5 (c)** and **(d)**, we see the interval of watermark embedding points can be scaled synchronously. Similarly, the watermark embedding points can also be translated synchronously with the whole image. In addition, the watermark bits hiding by the quantization in each embedding point can tolerate change of gray-scale values in certain extent, so our watermarking scheme can also survive other common image processing attacks such as JPEG compression, adding noise, median filtering, and histogram equalization.

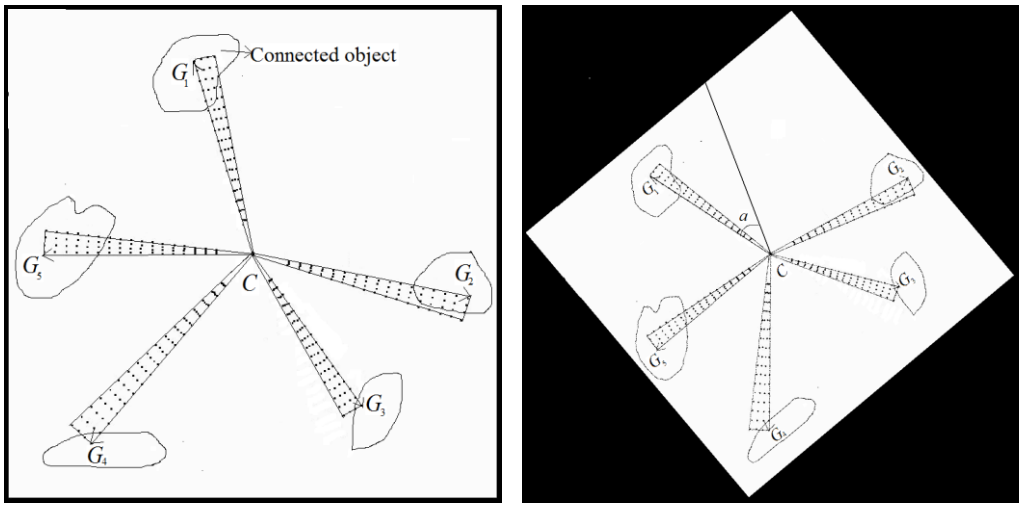

(a) Watermark embedding locations in five sectors **(b)** Rotation *a* degree

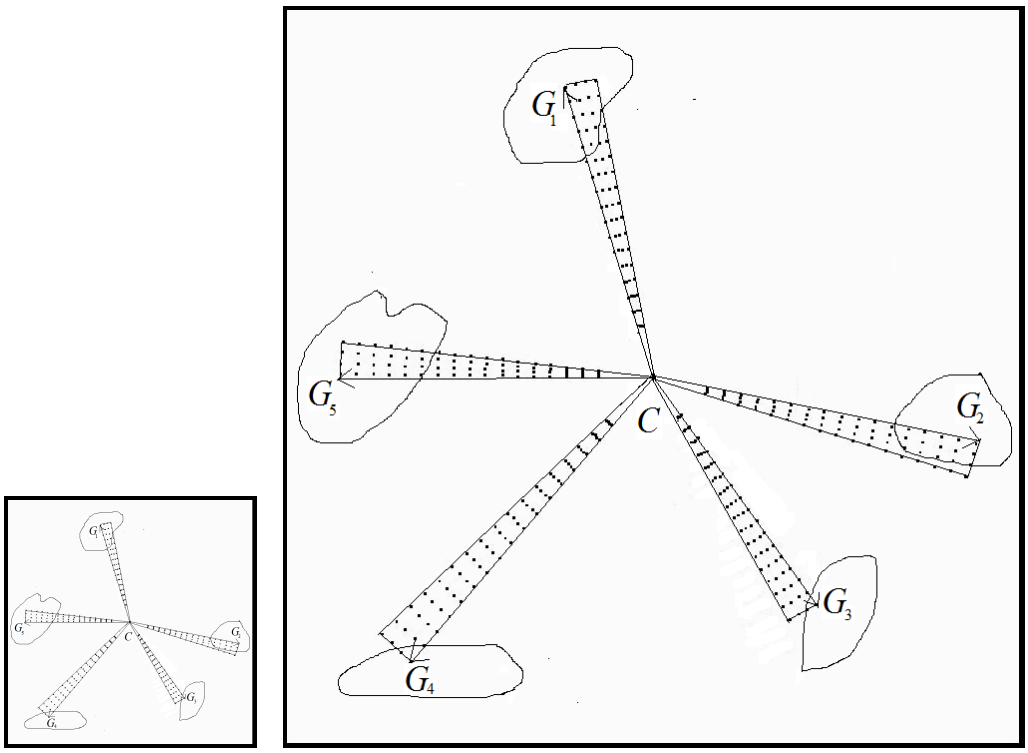

(c) 0.5 Scaling factor **(d)** 1.5 Scaling factor

Fig. 5. Sketch map of the watermark embedding locations under image rotation and scaling

5. Experimental Results

To evaluate the performances of the proposed scheme, we used the standard gray-scale image of size 512×512 ‘Lena’ and ‘Barbara’ as the test images shown in **Fig. 6**. In the test, the

window size of median filtering is set to 15×15, and T_1 is set to 0.79 for 'Lena', and 0.82 for 'Barbara', respectively. Then, we obtain the corresponding moderate connected components under 8-connectedness pattern shown in **Fig. 7**. When T_2 is set to 230, we can get six connected objects for 'Lena', and eight connected objects for 'Barbara', and then we calculate the gravity center coordinates of connected objects. They are (373,477), (35, 431), (146, 390), (456, 354), (234, 330), (105, 295) and (38, 298), (156, 229), (193, 194), (175, 181), (175, 144), (261, 132), (253, 71), (206, 84) for 'Lena' and 'Barbara', respectively. Set α =10°, we can obtain the corresponding sectors for watermark embedding based on these gravity centers of connected objects and the center of the whole image.

(a) Lena **(b)** Barbara

Fig. 6. Original image

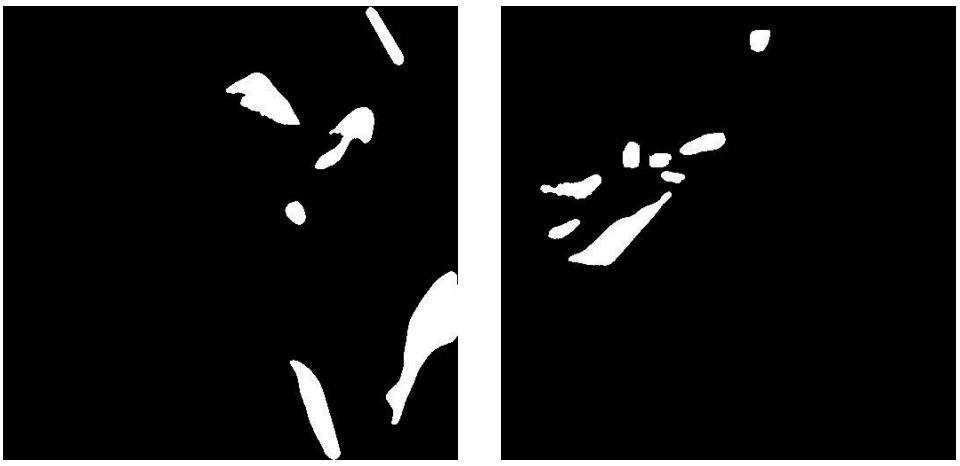

(a) Lena **(b)** Barbara

Fig. 7. Moderate connected objects

We embed the same version of 512-bit watermarks into each sector, and obtain the watermarked image. For a good watermarking scheme, the PSNR values of watermarked image should be greater than 36 dB, which is an experiential value. In this paper, the quantization step can be selected to meet the invisibility and robustness for watermarking application. Set the quantization step Δ =16, the resulting peak-signal-to-noise ratio (PSNR)

due to watermark embedding is calculated. The PSNR values between the original and watermarked images are 50.72dB and 53.80dB for 'Lena' and 'Barbara', respectively, indicating that invisibility of the watermark is satisfactory. **Table 1** shows the invisibility performance comparison between our scheme and other feature-based geometrically invariant watermarking schemes.

Table 1. PSNR(dB) for various watermarking schemes

Images	Li [11]	Wang [12]	Niu [15]	Our
Lena	42.57	36.10	40.57	50.72
Barbara	41.96	35.55	40.71	53.80

The robustness of the proposed scheme is demonstrated under both geometrical distortion and common image processing operations. Rotation, scaling and cropping are tested for geometrical distortion, while median filtering, adding Gaussian noise, JPEG compression, and histogram equalization are tested for common image processing operations. In this paper, the robustness is measured as the bit error rate (BER) of extracted watermark. For the extracted watermark $W' = \{w'_1, w'_2, \cdots \quad \in \{0,1\}\}$ and the original watermark $W = \{w_1, w_2, \cdots \quad \in \{0,1\}\}$, BER is defined as

$$BER = \frac{1}{n}\sum_{i=1}^{n}\left|w'_i - w_i\right| \tag{21}$$

Obviously, a low BER indicates that the extracted watermark has a stronger robustness. In the proposed scheme, the same version of watermarks is embedded into each sector, thus there are multi-version watermarks are extracted, and the lowest BER value of multi-version watermarks is as the valid BER value.

To examine the invariance against geometrical attack, we perform some geometrical attacks on 'Lena' and 'Barbara' images, respectively. As an example, **Fig. 8** shows some geometrically attacked 'Lena' images such as rotation, scalling and cropping. The watermark can be detected after the watermarked image suffered geometrical attacks. In order to demonstrate the robustness advantages of the proposed scheme, the watermark detection results are compared with methods [11][12][15], which are all feature-based geometrically invariant watermarking schemes.

(a) 10^o rotation **(b)** 80^o rotation

(c) 0.5 scaling factor **(d)** 1.5 scaling factor

(e) Cropping (H 20%, V 20%) **(f)** Cropping (H 50%, V 50%)

Fig. 8. Several geometrical attacked 'Lena' images

Fig. 9~**Fig. 12** show the simulation results under image rotation, scaling, cropping, and JPEG compression respectively. It is seen from **Fig. 9** that both the proposed method and the methods [11][12][15] can survive under different rotation degrees. For the proposed method, the BERs are extremely low, and the watermark can be accurately extracted regardless of rotation degrees. The reason is that when the watermarked image is rotated, the shapes of connected objects are invariable, so the gravity center of each connected object will be located synchronously with any rotation degrees. In this regard, the proposed scheme outperforms the

methods [11][12][15].

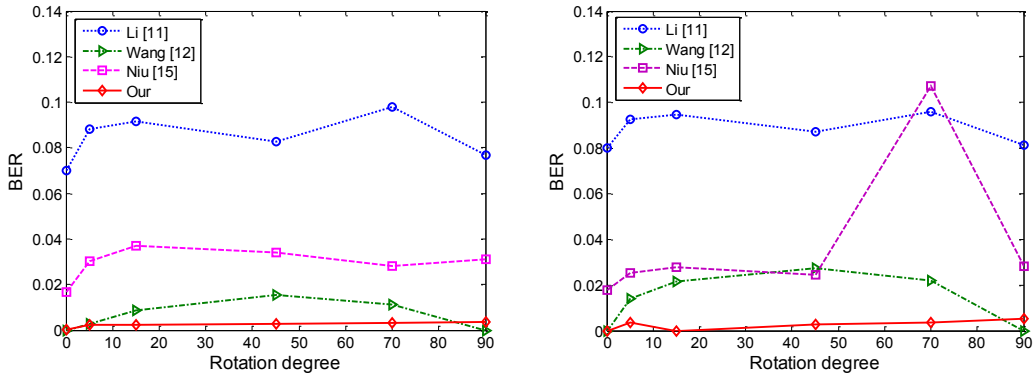

(a) Lena **(b)** Barbara

Fig. 9. Watermark detection results under different rotation degree

When the watermark image suffer scaling attack, the size of connected objects will be scaled synchronously following the image, and the reference length is scaled synchronously. Thus the watermark detection will be synchronized for scaling on the watermarked image. From **Fig. 10**, we know that both methods can resist scaling attacks. Especially, we find that when the image is scaled greater, the proposed method performs better, and the BERs are lower than that of the methods [11][12][15]. The underlying reason is that the connected objects are magnified, and gravity centers (feature points) are more stable, so the BERs are lower, and the extracted watermarks are more robust. On the contrary, in the case that an image is diminished, the stability of the feature points may be gone down when the related objects disappear. Therefore, the BERs will be risen. Although the BERs are higher than other three watermarking schemes when the scaling factor is less than 1, the proposed scheme is effective. By comparison, the overall performance of the proposed method is better than that of methods [11][12][15].

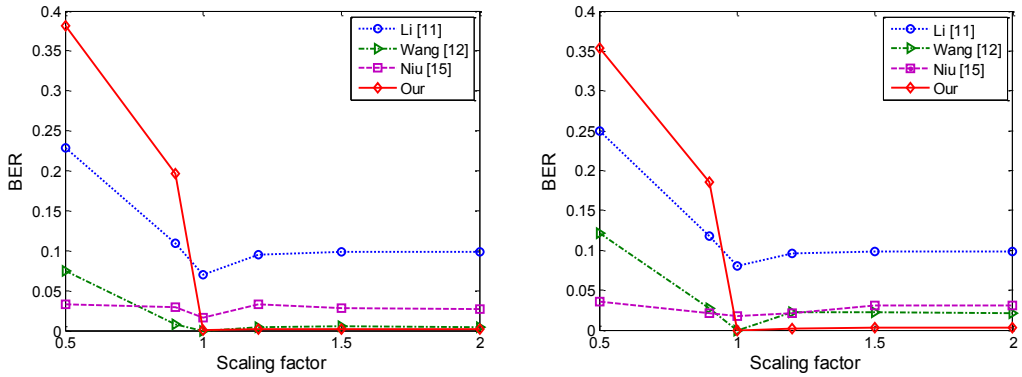

(a) Lena **(b)** Barbara

Fig. 10. Watermark detection results under different scaling factor

Cropping attack is a kind of local geometrical distortion. **Fig. 11** shows the watermark detection results under cropping attack. From **Fig. 11**, we see that the BERs of our scheme are the lowest, which implies that our scheme resists cropping attack well. However, the method

[11] cannot deal with image cropping, because Polar Harmonic Transforms is a statistical based image feature extraction method.

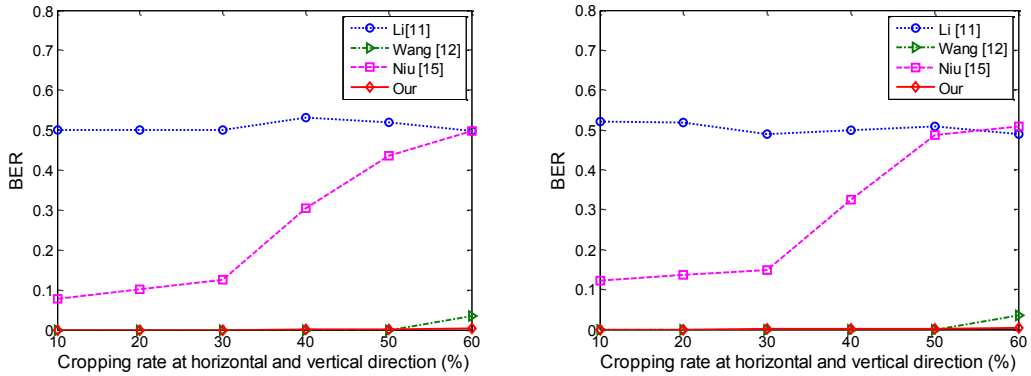

(a) Lena **(b)** Barbara

Fig. 11. Watermark detection results under cropping attack

In our scheme, the same version of watermarks is embedded into each sector, and the lowest BER value of all the extracted watermark versions is as the valid BER value. Even if only one extracted watermark version is well extracted under different attacks, the proposed scheme will be still valid and robust. As an example, we embed the same version of 512-bit watermarks into each sector formed by the connected objects in **Fig. 7(b)**. If the image 'Barbara' is cropped by (H 50%, V 50%) like **Fig. 8(f),** two gravity centers of the corresponding connected objects are still remained shown in **Fig. 12**. So the lowest BER value of two extracted watermark versions is as the valid BER result. In addition, the connectedness and gravity center of the image are stable to the cropping attack, so the BER values are low shown in **Fig. 11(b)**.

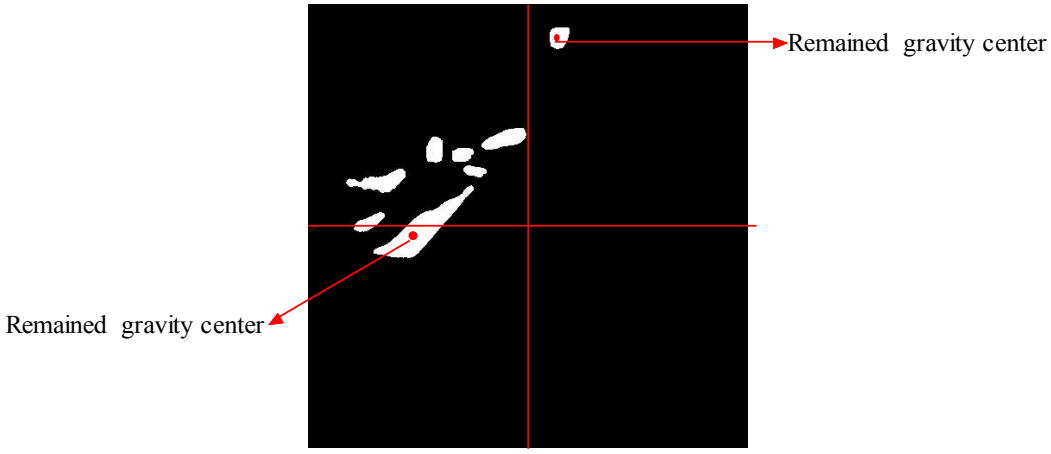

Fig. 12. Two gravity centers of 'Barbara'are still remained under cropping attack (H 50%, V 50%)

JPEG compression is a kind of common image processing operation. **Fig. 13** shows the watermark detection results under JPEG compression. From **Fig. 13**, we know that both methods can extract the watermark with high accuracy when the quality factors are greater than 30. Therefore, these methods are all robust to JPEG compression. In addition, the

watermark detection results under other common image processing operations are listed in **Table 2**.

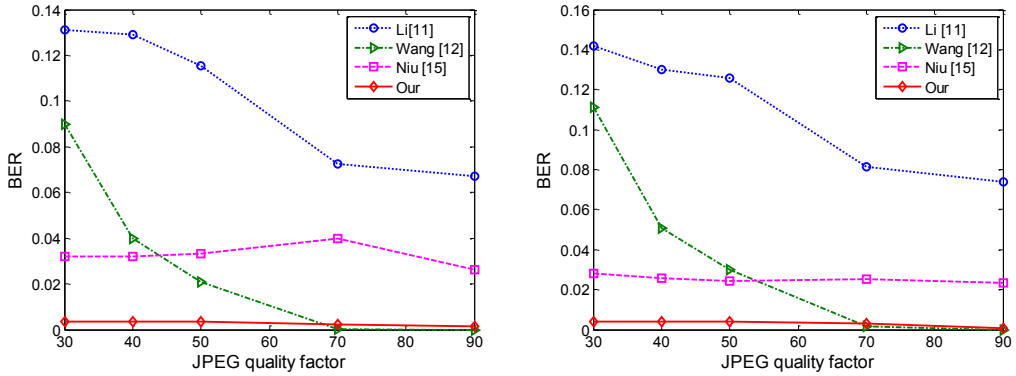

(a) Lena **(b)** Barbara

Fig. 13. Watermark detection results under JPEG compression

To sum up, the robustness to most geometrical attacks and common image processing operations is ensured because the connectedness and gravity center of the image is beneficial to immune to the considered attacks. In addition, If the rotation angles for forming the sectors are unknown, the watermark embedding location will not found by the illegal user. Consequently, the embedded watermark information is secure. Furthermore, as long as the connected objects are intact, their gravity centers will be not destroyed, and the extracted watermark will also be survived under local geometrical attacks. The experimental results show that the proposed scheme has a great improvement in the performance of extracted watermarks compared with the previous feature-based watermarking schemes.

Table 2. Watermark detection results under common image processing operations (BER)

Attacks	Lena				barbara			
	Li [11]	Wang [12]	Niu [15]	Our	Li [11]	Wang [12]	Niu [15]	Our
Median filter (3×3)	0.2031	0.0100	0.0264	0.0028	0.1358	0.0493	0.0304	0
Gaussian noise (0.05)	0.0781	0.0522	0.0273	0.0050	0.0814	0.0620	0.0215	0.0049
Histogram equalization	N/A	0.0002	0.0306	0	N/A	0.0105	0.0469	0.0003
Median filter (3×3)+JPEG 70	0.2886	0.0652	0.0273	0.0030	0.1850	0.1174	0.0218	0.0038

6. Conclusions

In this paper, we have presented a robust geometrically invariant watermarking scheme by using the connected object and gravity center of the digital image. The irregular connected

objects contact tightly with the spatial image content, which is changed adaptive synchronously with the image. We use the gravity centers of connected objects to be as the feature points for watermarking synchronization purpose, and improve the robustness to geometrical attacks. The experimental results demonstrate the proposed watermarking scheme is robust to most geometrical attacks, such as rotation, scaling and cropping, etc, and can also resist common image processing operations.

References

[1] M. H. Deng, Q. S. Zeng and J. Q. Yang, "A robust image watermarking algorithm based on HHT," *Procedia Engineering*, vol. 15, pp. 1544-1549, 2011. Article (CrossRef Link).

[2] H. Y. Yang, X. Y. Wang and L. L. Chen, "Geometrically invariant image watermarking using SVR correction in NSCT domain," *Computers and Electrical Engineering*, vol. 37, no.5, pp. 695-713, 2011. Article (CrossRef Link).

[3] L. D. Li, J. S. Qian and J. S. Pan, "Characteristic region based watermark embedding with RST invariance and high capacity," *International Journal of Electronics and Communications (AEü)*, vol. 65, no. 5, pp. 435-442, 2011. Article (CrossRef Link).

[4] J. C. Yen, "Watermark embedded in permuted domain," *IEE Electronics Letters*, vol. 37, no. 2, pp. 80-81, 2001. Article (CrossRef Link).

[5] H. X. Wang, H. Chen and K. Ding, "Public watermarking based on chaotic map," *IEICE Transactions on Fundamentals*, vol. E87-A, no. 8, pp. 2045-2047, 2004. Article (CrossRef Link).

[6] Z. J. Wang and R. K. Ward, "Robust image watermarking based on multiscale gradient direction quantization," *IEEE Transactions on Information Forensics and Security*, vol. 6, no. 4, pp. 1200-1213, 2011. Article (CrossRef Link).

[7] L. D. Li, X. P. Yuan, Z. L. Lu and J. P. Pan, "Rotation invariant watermark embedding based on scale-adapted characteristic regions," *Information Sciences*, vol. 180, no. 15, pp. 2875-2888, 2010. Article (CrossRef Link).

[8] S. Pereira and T. Pun, "Robust template matching for affine resistant image watermarks," *IEEE Transactions Image Processing*, vol. 9, no. 6, pp. 1123-1129, 2000. Article (CrossRef Link).

[9] A. R. Manuel and P. G. Fernando, "Analysis of pilot-based synchronization algorithms for watermarking of still images," *Signal Processing: Image Communication*, vol. 17, no. 8, pp. 611-633, 2002. Article (CrossRef Link).

[10] C. Y. Lin, M. Wu, J. A. Bloom, I. J. Cox, M. L. Miller and Y. M. Lui, "Rotation, scale and translation resilient watermarking for images," *IEEE Transactions Image Processing*, vol.10, no.5, pp. 767-782, 2001. Article (CrossRef Link).

[11] L. D. Li, S. S. Li, A. Abraham and J. S. Pan, "Geometrically invariant image watermarking using Polar Harmonic Transforms," *Information Sciences*, vol. 199, no. 15, pp. 1-19, 2012. Article (CrossRef Link).

[12] X. Y. Wang, C. P. Wang, H. Y. Yang and P. P. Niu, "A robust blind color image watermarking in quaternion Fourier transform domain," *The Journal of Systems and Software*, vol. 86, no. 2, pp. 255-277, 2013. Article (CrossRef Link).

[13] I. Nasir, F. Khelifi, J. Jiang and S. Ipson, "Robust image watermarking via geometrically invariant feature points and image normalisation," *IET Image Processing*, vol. 6, no. 4, pp. 354-363, 2012. Article (CrossRef Link).

[14] J. S. Tsai, W. B. Huang, Y. H. Kuo and M. F. Horng, "Joint robustness and security enhancement for feature-based image watermarking using invariant feature regions," *Signal Processing*, vol. 92, no. 6, pp. 1431-1445, 2012. Article (CrossRef Link).

[15] P. P. Niu, X. Y. Wang, Y. P.Yang and M. Y. Lu, "A novel color image watermarking scheme in nonsampled contourlet-domain," *Expert Systems with Applications*, vol. 38, no. 3, pp. 2081-2098, 2011. Article (CrossRef Link).

[16] F. N. Lang, J. L. Zhou, S. Cang, H. N. Yu and Z. W. Shang, "A self-adaptive image normalization and quaternion PCA based color image watermarking algorithm," *Expert Systems with*

Applications, vol. 39, no. 15, pp. 12046-12060, 2012. Article (CrossRef Link).
[17] T. Agui, H. Takahashi and H. Nagahashi, "Recognition of handwritten katakana in a frame using moment invariants based on neural network", *IEEE International Joint Conference on Neural Networks*, vol. 1, pp. 659-664, Nov. 1991. Article (CrossRef Link).
[18] R. C. Gonzalez and R. E. Woods, "Digital image processing", Pearson Education Inc., Prentice Hall, 2002. Article (CrossRef Link).

Hongxia Wang received the B.S. degree from Hebei Normal University, Shijiazhuang, in 1996, and the M.S. and Ph.D. degrees from University of Electronic Science and Technology of China, Chengdu, in 1999 and 2002, respectively. She engaged in postdoctoral research work in Shanghai Jiaotong University from 2002 to 2004. Currently she is a professor with School of Information Science and Technology, Southwest Jiaotong University, Chengdu. Her research interests include multimedia information security, digital forensics, information hiding and digital watermarking. She has published 50 peer research papers and wined 8 authorized patents.

Bangxu Yin received the B.S. and M.S. degrees from Southwest Jiaotong University, Chengdu, in 2006 and 2011, respectively. He is currently pursuing the Ph. D. degree with Southwest Jiaotong University. His research interests include multimedia information security and network security.

Linna Zhou received the Ph.D. degrees from Beijing University of Posts and Telecommunications, Beijing, in 2007, and then she engaged in postdoctoral research work in Tsinghua University. Currently she is a researcher. Her research interests include multimedia information security, digital forensics, and information hiding. She has published 30 peer research papers.